Turkish Journal of Science & Technology
15(2), 49-60, 2020

A Control of SynRM using MPPT Algorithm and Effects of Advance Angle on Motor Performance

Gullu BOZTAS[1*], Omur AYDOGMUS[2], Hanifi GULDEMIR[3]
[1,3]Electrical and Electronic Engineering, Technology Faculty, Firat University, Elazig, Turkey
[2]Mechatronics Engineering, Technology Faculty, Firat University, Elazig, Turkey
[*1]gboztas@firat.edu.tr, [2]oaydogmus@firat.edu.tr, [3]hguldemir@firat.edu.tr

(Geliş/Received: 26/03/2020; Kabul/Accepted: 30/07/2020)

Abstract: Solar-powered irrigation systems are quite important in terms of renewable energy usage. These systems consist of solar panel, boost converter, battery, battery charge management system, motor drive, motor and pump. The installation costs of system increase and the system reliability reduces due to the amount of equipment. Nowadays, low-voltage Permanent Magnet Synchronous Motors (PMSMs) are used to eliminate drawbacks of the boost converter. However, PMSMs have high cost because of the magnets. Synchronous Reluctance Motors (SynRMs) having lower cost than PMSMs can be used in these applications. The proposed system can be operated by using only the solar-panel, SynRM and drive without other devices. Thus, the system cost can be significantly reduced. In addition, durability of the system can be increased due to not using battery and magnets causing problems such as maintenance and low lifespan. A SynRM pump motor which can operate with a lower voltage level generated by the photovoltaic (PV) panel was designed in this paper. This motor has high efficiency because of no-copper losses of the rotor. Effects of advance angle on designed motor performance were analyzed and suitable advance angle was selected for the motor. Additionally, the designed SynRM was controlled by the MPPT algorithm.

Key words: AC Motors, Energy Conversion, Energy Efficiency, Solar Energy, Advance Angle, SynRM

MPTT Algoritması Kullanarak SynRM'nin Kontrolü ve İlerleme Açısının Motor Performansı Üzerindeki Etkileri

Öz: Güneş enerjisiyle çalışan sulama sistemleri, yenilenebilir enerji kaynak kullanımı açısından oldukça önemlidir. Bu sistemler güneş paneli, yükseltici çevirici, batarya, batarya şarj yönetim sistemi, motor sürücü, motor ve pompadan oluşur. Bu sistemlerde kullanılan ekipman miktarından dolayı sistem maliyeti artar ve sistem güvenirliği azalır. Günümüzde yükseltici çeviricinin dezavantajlarını ortadan kaldırmak için düşük gerilim seviyeli Sabit Mıknatıslı Senkron Motorlar (SMSM) kullanılır. Fakat kalıcı mıknatıslardan dolayı SMSM'ler yüksek maliyeti sahiptir. Senkron Relüktans Motorlar (SynRM), SMSM'lerden daha düşük maliyete sahiptir. Önerilen sistem; sadece güneş paneli, SynRM ve motor sürücüsü kullanılarak gerçekleştirilebilir. Böylece sistem maliyeti önemli ölçüde azaltılabilir. Ayrıca bakım ve düşük kullanım ömrü gibi sorunlara neden olan batarya ve mıknatısların kullanılmaması nedeniyle sistemin dayanıklılığı arttırılabilir. Bu çalışmada; Fotovoltaik (FV) panel tarafından üretilen düşük gerilim seviyesinde çalışabilen bir pompa motoru tasarlanmıştır. Tasarlanan motor rotorunda bakır kayıpları olmamasından dolayı yüksek verime sahip olan SynRM olarak tasarlanmıştır. Tasarlanan motor performansı üzerinde ilerleme açısının etkileri incelenmiştir ve motor için uygun ilerleme açısı seçilmiştir. Ayrıca tasarlanan SynRM, MPPT algoritması ile birlikte kontrol edilmiştir.

Anahtar kelimeler: AA Motorlar, Enerji Dönüşümü, Enerji Verimi, Güneş Enerjisi, İlerleme açısı, SynRM

1. Introduction

Nowadays, global warming and energy policies have become an important issue on the international agenda. Greenhouse gas emissions have been reduced by developed countries. PV system has become an important renewable source because it can generate electricity without emitting greenhouse gasses [1]. In addition, PV panels are a suitable solution for areas far from the electric source. The efficiency of the PV power stations has three factors such as the efficiency of the PV panel (8-15%), the efficiency of the inverter (95-98%) and efficiency of the Maximum Power Point Tracking (MPPT) (98%) [2]. Nowadays, the efficiency of the PV panels is reached up

[*] Corresponding author: gboztas@firat.edu.tr. ORCID Number of authors: [1]0002-1720-1285, [2]0001-8142-1146, [3]0003-0491-8348

only 22% by very few producer firms (Panasonic, SunPower, etc.). MPPT is an important parameter in order to obtain desired maximum power in the PV systems. MPPT algorithms must be used in the PV systems because PV panel arrays have a nonlinear voltage-current (V-I) characteristic with only one maximum point. This point depends on irradiation conditions and panel temperature changed by weather through both days and seasons. There are nearly 20 different MPPT algorithm in the literature [3–5]. Perturb and Observe (P&O) and Incremental Conductance (InCond) are more widely used than other algorithms. In addition, there are MPPT algorithms such as fuzzy logic, artificial neural network, fractional open circuit voltage or short circuit current, current sweep.

Electric motors consume nearly 50% of total electrical energy. Especially, fan, pump and compressor motors constitute more than half of the consuming electrical energy of the motors [6]. Generally, three-phase induction motors are widely used in all of the motor applications. Therefore, numerous studies have been performed in order to increase the efficiency of the induction motors. Reduction gear systems and/or belt-pulley systems are generally used so as to obtain high torque from an induction motor at low speed region. However, these systems have low efficiency because of high friction. DC motors were preferred in low speed-high torque applications in the past. Brushless DC (BLDC) motor and PMSM have been used since 1980's. They do not require brush-collector and rotor winding. These motors known as synchronous motor have advantages such as high performance, low volume and high efficiency [7–9]. They have a major problem such as not available direct-starting with grid connected. Therefore, these motors require a motor drive. They have high costs because these motors have magnets on the rotor. Therefore, in nowadays, Synchronous Reluctance Motors (SynRM) have a rising trend because of not requiring any windings and magnets on the rotor. SynRM can produce shaft torque by using reluctance concept similarly sinusoidal rotating magnetic field generated from the stator of the traditional induction motor. The theoretical concept of reluctance torque was firstly presented by Kostko in 1923 [10]. SynRM has become popular thanks to developing power electronic drive systems with feedback control. Field Oriented Control (FOC), Direct Torque Control (DTC) and similar methods is presented in literature in order that SynRM can be operated [11–15].

Until nearly two decades ago, SynRMs were less preferred because they had higher torque ripples and lower average torque according to the other AC motors. The efficiency and torque of SynRMs are increased by developing of the motor design program. Nowadays, modern SynRMs can generate 15-20 % more torque than same-size induction motor [16,17]. Also, SynRMs have a lower power loss and higher torque according to induction motor at the same stator current. Both performance and efficiency of the SynRMs can be increased by using a motor drive. SynRMs may have unstable operation points when operated with a simple V/f control. Therefore, FOC or DTC is widely preferred in order to control speed of SynRMs. These control methods are required either rotor position or flux position information. Sensorless speed control methods are generally used instead of mechanical position encoders due to low cost and high robustness. DTC is simpler than FOC though most of researchers focus on FOC for sensorless motor drive [13,18–21]. Consoli and et al. are proposed sensorless torque control for SynRM drives. SynRMs are used in variable speed applications with high efficiency [16,22–24]. These motors are more superior than induction motors because of simpler of mass production, higher efficiency, higher density of torque [11,24] higher load capacity and lower rotor temperature. SynRMs have become popular due to these superior properties [25–27]. However, these machines require an inverter bigger than standard size inverter due to their low power factor (PF) [10]. The PF of SynRM can be increased by using rotor structure assisted Permanent Magnet (PM) which is known as Permanent Magnet Assisted SynRM (PMaSynRM) [11,28].

In this work, a pump motor was designed a SynRM directly connected to PV panels which generate a low voltage level. Robustness of SynRM rotor is higher than other motors because SynRM has not magnets and windings on its rotor. In addition, SynRM has constant efficiency and constant torque with independent speed. An MPPT algorithm was modified in order to continuously obtain maximum speed from the motor drive. This system has more efficiency, more compact and user friendly than other pump motor drive systems. Firstly, the effects of rotor shape were analyzed with 9 different types of the rotor in this paper. Then, optimal rotor type was analyzed with Finite Element Method by using Magnet/Infolytica. Effects of advance angle on performance of the designed motor were analyzed and suitable advance angle was selected for the motor. The proposed system can be operated by using only the solar-panel, selected optimal SynRM and drive without battery, battery management system and boost converter. The current commercial system and proposed system are given in Figure 1.

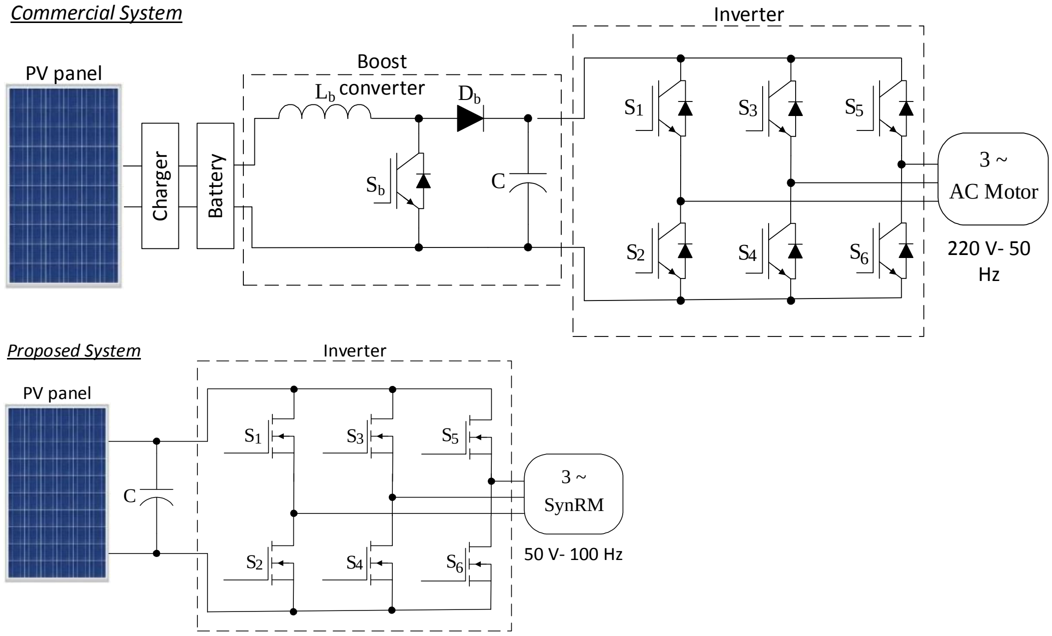

Figure 1. a) Commercial system, b) Proposed system with SynRM

Nowadays, pump systems which do not require battery, battery management system and boost converters are available in the market for PV systems. So far, SynRM has not been used for these pump systems in the market. The main contribution of this study is to obtain a high efficiency solar-based pump system instead of the traditional pump systems. Additionally, the purposed motor has a lower stator stack length and no copper losses on the rotor when compared with an induction motor.

2. Design of SynRM

In this paper, SynRM was designed as 30 slot stator and 4 barrier rotor. Other constant values of the motor parameters were taken in appendix. Rotor core has air barriers through the *q*-axis in order to both increase L_d inductance and decrease L_q inductance. Rotor rips were chosen as possible as narrow, so that flux generated in stator can be oriented to the rotor. Thus, the desired high reluctance torque was obtained. The outer diameter of designed motor was taken as 90 mm. Firstly, the effects of rotor shape were analyzed with 9 different types of the rotor in this paper. Barriers and rips of the rotor were arranged in order to show the effect on the motor performance of rotor shape. As shown in Figure 2, barriers, rips and iron bridge thickness of the rotors were named as ST, WT and BT, respectively. Besides, R_O and R_i are outer and inner radius of the rotor. Design parameters of the rotors are given in Table 1. All dimensions have been given in mm.

Table 1. Rotor Design Parameters

Design	ST1	ST2	ST3	ST4	WT1	WT2	WT3	WT4	WT5	T(Nm)
D1	2.82	2.03	1.27	1.04	2.38	2.92	1.79	2.08	4.70	**2.27**
D2	2.28	2.28	2.28	2.28	2.57	2.28	2.28	2.28	2.50	**2.22**
D3	2.94	2.90	2.90	2.90	2.57	1.45	1.45	1.45	2.50	**2.33**
D4	1.59	1.60	1.60	1.60	2.57	3.20	3.20	3.20	2.50	**2.10**
D5	3.06	2.82	2.58	2.35	2.57	1.56	1.72	1.88	2.50	**2.33**
D6	**3.62**	**3.04**	**2.47**	**1.90**	**2.57**	**1.26**	**1.65**	**2.03**	**2.50**	**2.29**
D7	3.08	2.46	1.84	1.23	2.57	3.07	2.46	1.84	2.50	**2.23**
D8	2.67	2.43	1.90	1.10	2.57	2.61	2.43	1.90	3.50	**2.23**
D9	3.89	3.52	2.50	1.11	2.17	2.42	2.42	2.42	0.50	**2.27**

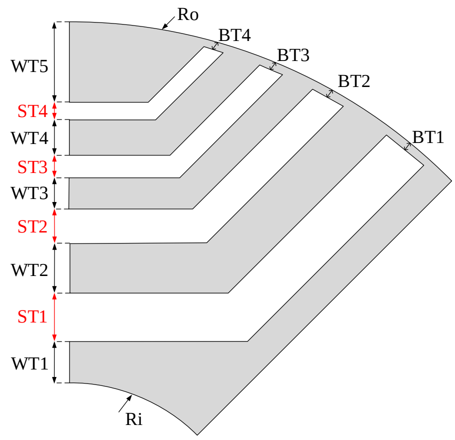

Figure 2. Rotor structure

The flux density distributions in the stator and the rotor of designed SynRMs are illustrated in Figure 3. The material of lamination was determined as M530-50. Additionally, speed-torque curves of the motors are given in Figure 4. Optimal rotor shape was determined by examining the flux density distributions and speed-torque curves. It can be said that all the structures of the designed motors have small differences with each other.

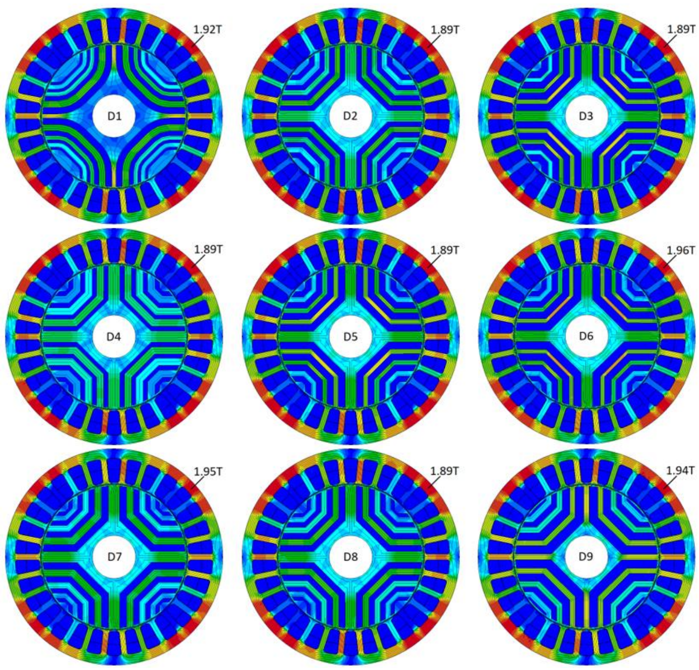

Figure 3. The flux density distribution of the designed motors

All designed motors are produced up to 2 Nm when the speed-torque curves of designed motor are compared each other as shown in Figure 4. It is observed that the flux in rotor types generating high torque is intensified throughout rotor rips. It is the right approach to make the rips as thin as possible in the rotor design. The flux of the D6 motor is more intensified than the other motors throughout rotor rips and D6 motor produces the highest flux according to others. Breakdown torque of the D6 motor is higher than other designed motors. Additionally, this motor has high torque at high speeds than the others. Therefore, D6 motor was selected as the most suitable motor to use in this paper, though average torque of the D6 motor is lower than D3 and D5 motors.

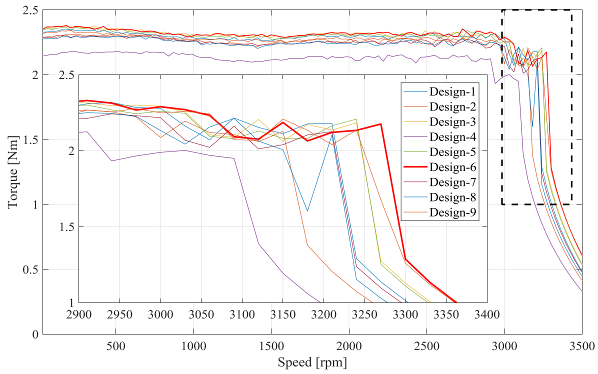

Figure 4. Speed-torque curves of the designed motor

The dimensions of the motor are shown in Table 1. It is aimed to operate in a constant torque region, which is between 0 and 3000 rpm. The advance angle is an important parameter in order to generate high torque. Effecting on the speed-torque curve of the advance angle is illustrated in Figure 5. It must be considered that the motor produces high torque at the nominal speed while the advance angle is determined. It can be seen that optimal advance angle of the motor is 54° as shown in Figure 5.

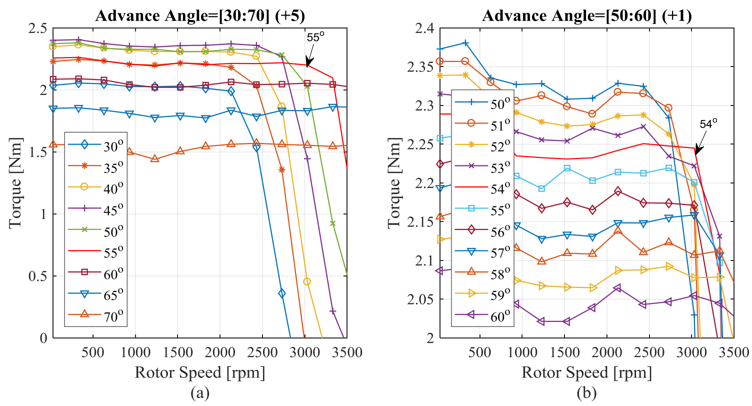

Figure 5. The effects on the speed-torque curve of the advance angle

D6 motor was analyzed with Finite Element Method (FEM)-Newton Raphson Iteration by using Magnet/Infolytica program. Maximum element size is 1 mm, maximum Newton iteration number is 50 and Newton iteration tolerance is 1% in FEM. Additionally, start, stop and step times have been taken as 0, 20 ms and 10 ms, respectively. The torque of the motor is shown in Figure 6. The motor produces nearly 2.4 Nm.

Mesh of the motor is given Figure 7a. Maximum element size of the mesh has been taken as 1 mm. The flux density distribution of the motor is obtained as illustrated in Figure 7b. The maximum motor flux is nearly 1.96 T.

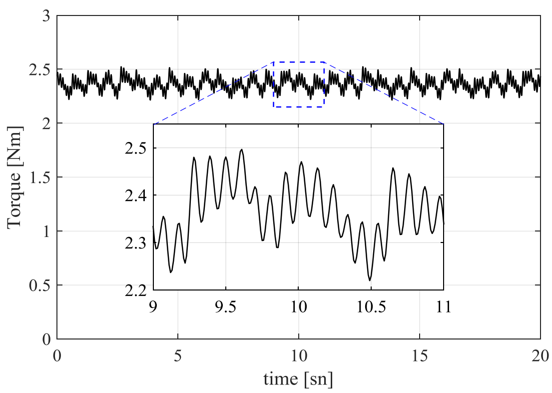

Figure 6. Torque curve of the optimal motor

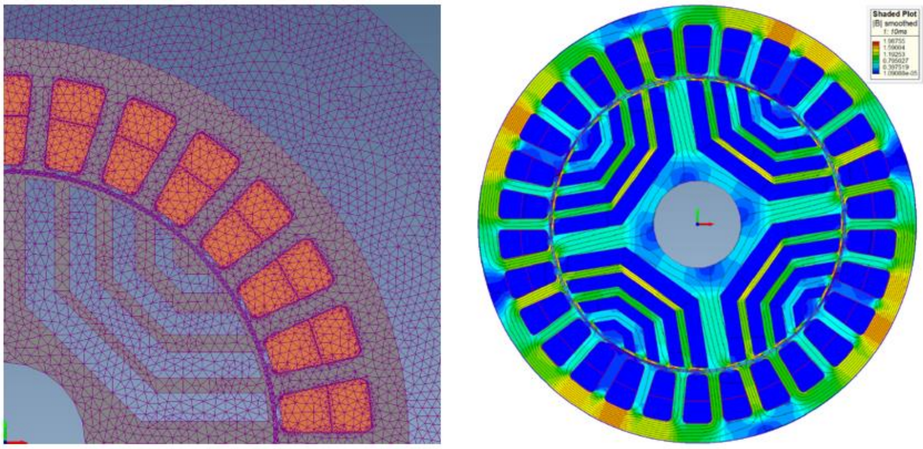

(a) (b)

Figure 7. a) Mesh of the motor, **b)** The flux density distribution

The curves of torque, output power, efficiency and PF according to speed are illustrated in Figure 8. The motor is operated in the constant torque region. The obtained torque as 2.3 Nm is kept up from standstill to steady-state. The efficiency of the motor is obtained as 86.4% at the nominal speed. Also, the efficiency is approximately 75% at the half of the nominal speed. Output power is 715 W at the rated speed. PF is a disadvantage for SynRMs. It can be shown that the PF factor is lower than the equal AC motors.

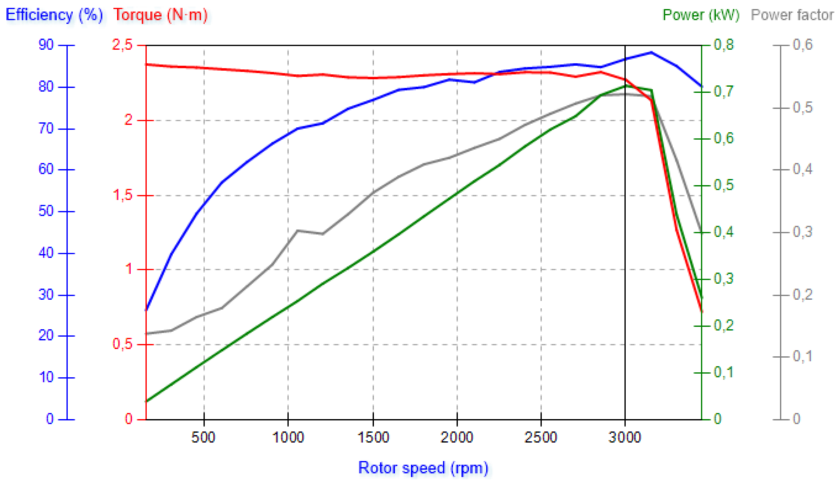

Figure 8. Torque, output power, efficiency and PF of SynRM

Parameters of designed SynRM are given in appendix. It shows that the value of K_t is zero because there is no magnet on the rotor. Increasing of the L_d/L_q is an important parameter in order to obtain high torque from motor. In this work, L_d/L_q is obtained as 3.74.

3. Control of SynRM

The SynRM has been controlled by using DTC algorithm and the control algorithm diagram is given in Figure 9. The stator flux vector plane ia divided into six sectors θ_1-θ_6. The switching logic of the traditional DTC is given in Table 2. This DTC algorithm needs information of the stator flux (λ_s) and the electromagnetic torque (T_e). The equations of torque and stator flux are given in Equations (1)-(4). The PI parameters of the speed controller are determined as k_p=0.25, k_i=5.

Table 2. Switching logic of the classical DTC

Sectors →		θ_1	θ_2	θ_3	θ_4	θ_5	θ_6
ξλ=1	*ξT=1*	V_2 (110)	V_3 (010)	V_4 (011)	V_5 (001)	V_6 (101)	V_1 (100)
	ξT=-1	V_6 (101)	V_1 (100)	V_2 (110)	V_3 (010)	V_4 (011)	V_5 (001)
ξλ=-1	*ξT=1*	V_3 (010)	V_4 (011)	V_5 (001)	V_6 (101)	V_1 (100)	V_2 (110)
	ξT=-1	V_5 (001)	V_6 (101)	V_1 (100)	V_2 (110)	V_3 (010)	V_4 (011)

$$\lambda_\alpha = \int \left(V_\alpha - i_\alpha R_s\right) dt \tag{1}$$

$$\lambda_\beta = \int \left(V_\beta - i_\beta R_s\right) dt \tag{2}$$

$$|\lambda_s| = \sqrt{\lambda_\alpha^2 + \lambda_\beta^2} \tag{3}$$

$$T_e = \frac{3}{2} P\left(\lambda_\alpha i_\beta - \lambda_\beta i_\alpha\right) \tag{4}$$

where λ_α and λ_β are flux of α and β axis, respectively. MTPA trajectory can be shown in Equation (5).

$$|\lambda s|^* = \sqrt{\frac{2}{3P} \frac{L_d^2 + L_q^2}{L_d - L_q} |T_e|^*} \tag{5}$$

where $|\lambda_s|^*$ and $|T_e|^*$ are stator flux reference and torque reference, respectively.

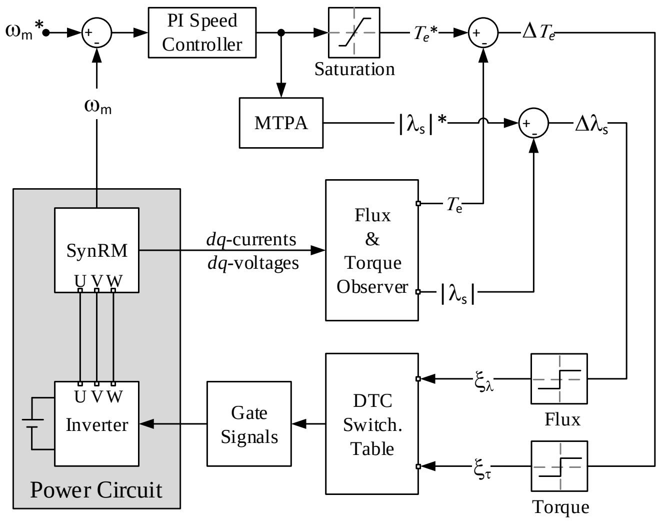

Figure 9. Block diagram of the SynRM control

MPPT algorithms are required for PV applications because the maximum power point (MPP) of the solar cells dependents on the unstable irradiation and temperature. Many MPPT algorithms are available in the literature. Perturb–Observe (P&O) and Incremental Conductance (IC) are widely used in nowadays. P&O algorithm is preferred as shown in Figure 10 in this study. The P&O algorithm has been modified for motor speed control. The reference motor speed is determined by using MPPT algorithm.

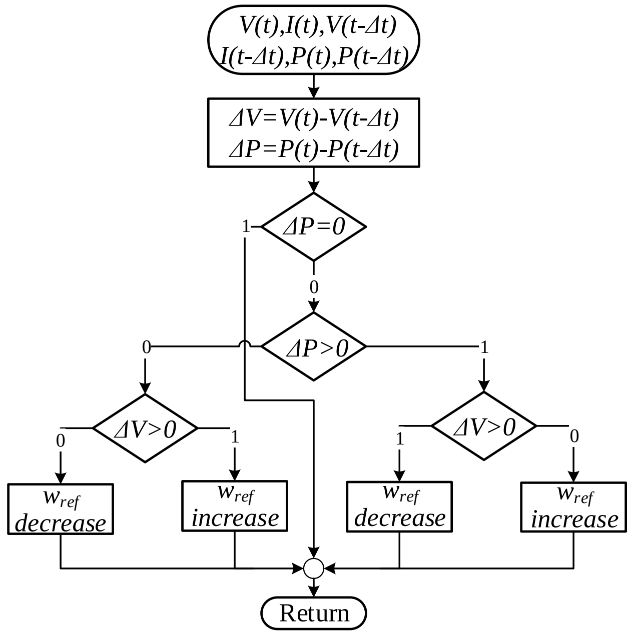

Figure 10. Modified P&O algorithm for the motor speed control

MPP is illustrated on V-I and V-P curves of the PV panel for different irradiation and temperature conditions in Fig. 11. The model of the PV panel having 2 series modules and 2 parallel strings is Soltech STH-245-WH. V-I and V-P curves of the PV panel are illustrated in Fig. 11a and Fig. 11b for 0.25 kW/m^2, 0.75 kW/m^2 and 1 kW/m^2 irradiation conditions at 25ºC. The panel current and power increase at MPP when irradiation value of the PV panel increases at the same temperature. Additionally, voltage and power of the panel decrease at MPP when the temperature value of the PV panel increases at the same irradiation condition as shown in Fig. 11c and Fig. 11d.

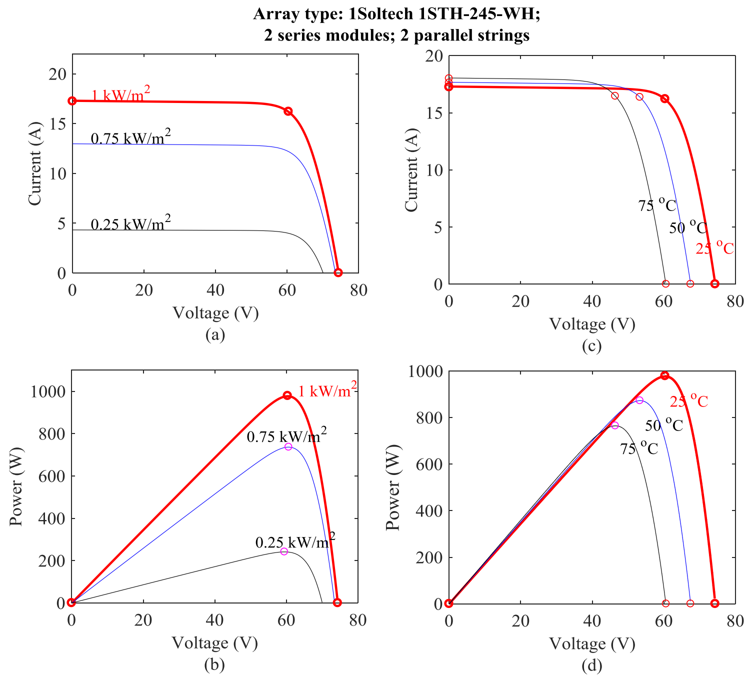

Figure 11. V-I and V-P curves of the PV panel for; **a/b)** different irradiation at 25ºC **c/d)** different temperature at 1kW/m^2

4. Simulation Results

The system consisting of MPPT, power circuit and DTC blocks is performed by using MATLAB as shown in Figure 12. MPPT algorithm determines the speed demanded for the operation of the SynRM by calculating MPP. Thus, the SynRM can be operated at the MPP via DTC. The simulation blocks are separated as digital and real systems to obtain close to real results. The sample time of the digital system is taken as 10 μs. The real system simulation blocks have 1 μs sample time. Therefore, the separated systems are connected via rate-transition block which is supported with MATLAB.

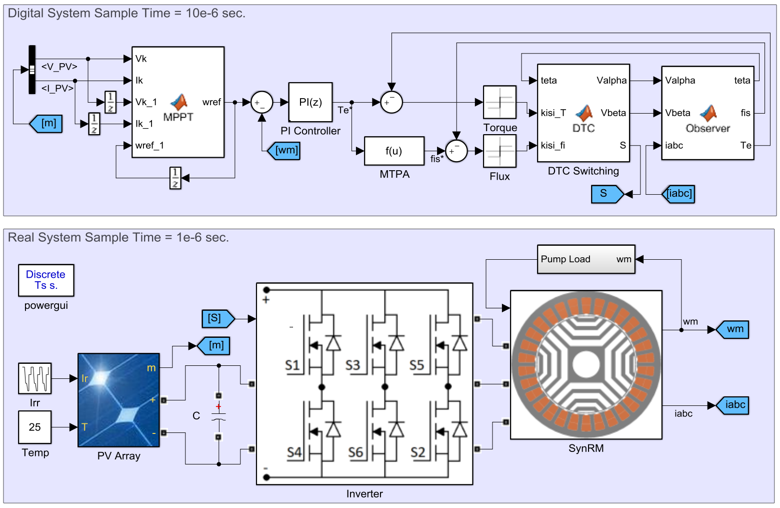

Figure 12. Control blocks of SynRM directly fed PV panel with MPPT algorithm

The system is tested for different irradiation conditions to analyze motor drive system having MPPT algorithm. Voltage, current and power of the PV panel have changed according to variation of the irradiation value at 25°C as shown in Figure 13 and Figure 14. The power of the motor must be reduced as PV panel power decreases. For this reason, the motor control system must be aware of these variable conditions. If this is not achieved, the motor synchronization will fail because enough power is not provided to motor. The results are illustrated to show the performance of the motor, DTC and MPPT under 25°C temperature and variable irradiation conditions in Figure 13.

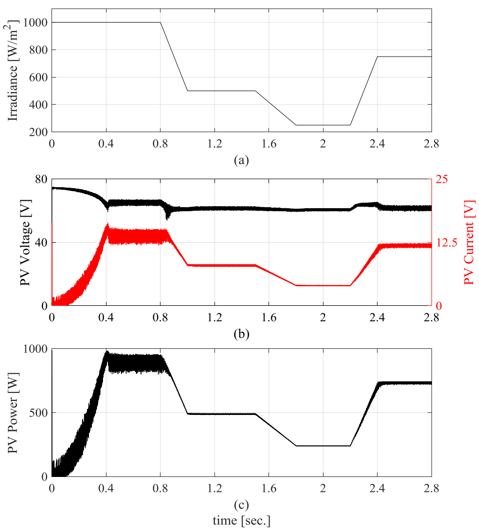

Figure 13. a) Irradiation conditions, **b)** I and V curves, **c)** PV Power

Three-phase stator currents, speed and electromagnetic torque of the motor are analyzed. Three-phase currents, nominal speed, frequency and produces torque of the motor are decreased when irradiation value decreases and vice versa. The detailed current waves are given in Figure 14a. It can be seen that the frequencies of the currents are changed according to motor reference speed. The motor speed is changed by the MPPT algorithm and the desired power rating of the motor is provided from the PV panels when the irradiation conditions change. In this study, the load torque is proportionally adjusted by motor speed.

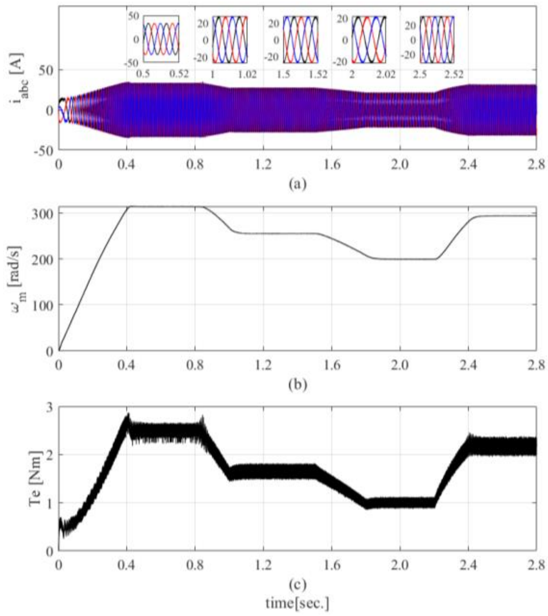

Figure 14. a) Stator currents**, b)** Motor speed, **c)** Electromagnetic torque

5. Conclusion

The majority of electrical energy is consumed by electric motors in industrial and other applications. The pump motor is the overriding of motor types used in industry. The increasing of pump motor efficiency plays an important role in the total energy consumption. The pump speed is so an important parameter to obtain high efficiency in the pump systems. Induction motors have lower speed than synchronous motors under the same conditions because induction motors have a slip between the angular speed of generated magnetic field and angular speed of the rotor. Therefore, using a synchronous motor is a better solution than an induction motor in order to obtain high speed and efficiency for pump systems.

In this paper, a SynRM and a drive system were developed as an alternative to the available systems to provide maximum benefit from the solar energy which is a renewable energy source. Firstly, 9 different motor were designed for this purpose. Rotor shapes of the designed 9 different motors are different each other while stator structures of these motors are same. Then, the effects of rotor shape were analyzed with 9 different rotor types. Barriers and rips of the rotor were changed in order to show the effect on the motor performance of rotor shape and performance curves of the designed motor were analyzed. As a result of the analysis, motor producing 2.3 Nm was selected for this study. Effects of advance angle on designed motor performance were analyzed and advance angle was selected as 54°for this motor. Output power, efficiency and torque of this motor are 715W, 86.4% and 2.3 Nm at rated speed. DTC and MPPT algorithms were used for motor drive system and 3-phase current, angular speed and torque have been analyzed. The efficiency of the designed SynRM is about 86% while the efficiency of a commercial 3-phase induction motor is about 71% for pump. Additionally, the stack length of the designed motor was obtained as 110 mm while stack length of the induction motor is 150 mm for the standard pump motor. Advantages of this work are given as follows; increasing efficiency of the solar pump system, reducing length of the stator stack according to induction motor, eliminating copper losses of the rotor, reducing the cost of the system, reducing the amount of devices (boost converter, magnet, battery, charger) used in the traditional pump systems. Consequently, a novel design is proposed as an alternative system to the low power solar pump systems instead of the traditional systems in this study.

Appendix A

dq-parameters of designed SynRM

K_t (Torque over RMS phase current) 0 N.m/A, L_d (d-axis inductance) 2.1 mH, L_q (q-axis inductance) 0.561 mH, L_d/L_q (aligned/unaligned) 3.74, L average1.33 mH, R_s (Stator phase resistance) 0.0602 Ω, I_{rms} (RMS current) 23.

Appendix B

Motor parameter values

Supply voltage 50 V, Rated current 23 A, Rated speed 3000 rpm, Rated frequency 100 Hz, Pole number 4, Number of phases 3, Number of slots 30, Outer diameter of the stator 90 mm, Air gap thickness 0.5 mm, Stack height 110 mm, Outer diameter of the rotor 60 mm, Inner diameter of the rotor 18 mm.

Acknowledgment

The authors would like to thank The Scientific and Technological Research Council of Turkey (TUBITAK) for financial support (Project No: 116E116)

References

[1] Kostko JK. Polyphase reaction synchronous motors. J Am Inst Electr Eng 1923; 42: 1162–1168.
[2] Lagerquist R, Boldea I, Miller TJE. Sensorless-control of the synchronous reluctance motor. IEEE Trans. Ind. Appl 1994; 30: 673-682.
[3] Xu L, Xu X, Lipo TA, Novotry DW. Vector Control of a Synchronous Reluctance Motor Including Saturation and Iron Loss. IEEE Trans Ind Appl 1991; 27: 977–985.
[4] Deniz E. ANN-based MPPT algorithm for solar PMSM drive system fed by direct-connected PV array. Neural Comput Appl 2017; 28: 3061–3072.
[5] Gündoğdu A, Güre B. Design, Construction and Implementation of Low Cost Photovoltaic Water Pumping System for Agricultural Irrigatin. Balk J Electr Comput Eng 2019:72–80.
[6] Aydogmus O. Design of a solar motor drive system fed by a direct-connected photovoltaic array. Adv Electr Comput Eng 2012; 12: 53–58.
[7] Kumar R, Singh B. Solar photovoltaic array fed water pump driven by brushless DC motor using Landsman converter. IET Renew Power Gener 2016; 10: 474–484.
[8] Aydogmus O, Deniz E, Kayisli K. PMSM Drive Fed by Sliding Mode Controlled PFC Boost Converter. Arab J Sci Eng 2014; 39: 4765–4773.
[9] Celikel R, Aydogmus O. A torque ripple minimization method for brushless DC motor in high speed applications using buck boost topology. J Eng Res 2019; 7: 200–214.
[10] Xu L, Xu X, Lipo TA, Novotry DW. Vector Control of a Synchronous Reluctance Motor Including Saturation and Iron Loss. In: Conference Record of the 1990 IEEE Industry Applications Society Annual Meeting; 7-12 Oct. 1990; Seattle, USA: IEEE. pp. 1–13.
[11] Piegari L, Rizzo R. Adaptive perturb and observe algorithm for photovoltaic maximum power point tracking. IET Renew Power Gener 2010; 4: 317-328.
[12] Femia N, Petrone G, Spagnuolo G, Vitelli M. Optimizing sampling rate of P&O MPPT technique. In: PESC Rec. - IEEE Annu. Power Electron. Spec. Conf., 20-25 June 2004; Aachen, Germany. pp. 1945–1949.
[13] Esram T, Chapman PL. Comparison of Photovoltaic Array Maximum Power Point Tracking Techniques. IEEE Trans Energy Convers 2007; 22: 439–449.
[14] Gao J, Wu X, Huang S, Zhang W, Xiao L. Torque ripple minimisation of permanent magnet synchronous motor using a new proportional resonant controller. IET Power Electron 2017; 10: 208–214.
[15] Shukla S, Singh B. Solar powered sensorless induction motor drive with improved efficiency for water pumping. IET Power Electron 2018; 11: 416–426.
[16] Hussein KH, Muta I, Hoshino T, Osakada M. Maximum photovoltaic power tracking: an algorithm for rapidly changing atmospheric conditions. Gener Transm Distrib IEE Proceedings- 1995; 142: 59–64.
[17] Gundogdu A, Dandil B, Ata F. Asenkron Motorun Histeresiz Denetleyici Tabanlı Doğrudan Moment Denetimi. Fırat Üniversitesi Mühendislik Bilim Derg 2017; 29: 197-205.
[18] Rahim NA, Che Soh A, Radzi MAM, Zainuri MAAM. Development of adaptive perturb and observe-fuzzy control maximum power point tracking for photovoltaic boost dc–dc converter. IET Renew Power Gener 2014; 8: 183–194.
[19] Rizzo SA, Scelba G. ANN based MPPT method for rapidly variable shading conditions. Appl Energy 2015; 145: 124–132.
[20] Elobaid LM, Abdelsalam AK, Zakzouk EE. Artificial neural network-based photovoltaic maximum power point tracking techniques: a survey. IET Renew Power Gener 2015; 9: 1043–1063.
[21] Noguchi T, Togashi S, Nakamoto R. Short-current pulse-based maximum-power-point tracking method for multiple photovoltaic-and-converter module system. IEEE Trans Ind Electron 2002; 49: 217–223.

[22] Staton DA, Miller TJE, Wood SE. Maximising the saliency ratio of the synchronous reluctance motor. IEE Proc B Electr Power Appl 1993; 140: 249-259.
[23] Lipo TA. Synchronous reluctance machines-a viable alternative for ac drives? Electr Mach Power Syst 1991; 19: 659–671.
[24] Kamper MJ, Van Der Merwe FS, Williamson S. Direct finite element design optimisation of the cageless reluctance synchronous machine. IEEE Trans Energy Convers 1996; 11: 547–553.
[25] Taghavi S, Pillay P. A Sizing Methodology of the Synchronous Reluctance Motor for Traction Applications. IEEE J Emerging Selected Topics in Power Elect. 2014; 2: 329-340.
[26] Ferrari M, Bianchi N, Doria A, Fornasiero E. Design of Synchronous Reluctance Motor for Hybrid Electric Vehicles. IEEE Trans. Ind. Appl., vol. 51, 2015, p. 3030–40. https://doi.org/10.1109/TIA.2015.2410262.
[27] Truong PH, Flieller D, Nguyen NK, Mercklé J, Sturtzer G. Torque ripple minimization in non-sinusoidal synchronous reluctance motors based on artificial neural networks. Electr Power Syst Res 2016; 140: 37–45.
[28] Moghaddam RR. Synchronous Reluctance Machine (SynRM) Design. MSc, Royal Institute of Technology, Stockholm, 2007.